Chapter 10

Bifurcation Effects Generated with Holographic Rough Surfaces

G. Martínez Niconoff, G. Díaz González,
P. Martínez Vara, J. Silva Barranco and
J. Munoz-Lopez

Additional information is available at the end of the chapter

http://dx.doi.org/10.5772/54512

1. Introduction

The holographic research is related to the coded storage and the ulterior decoded of optical information [1]. The holographic processes involved had extended its application to almost all the optical areas; such that nowadays is not possible to conceive the development of the modern optics without this powerful tool [2-5]. The development of this area implies the generation of optical fields with suitable structure also as the research and synthesis of novel holographic materials with large refractive index values and sensible to a wide frequencies range [6-8].

In the present study, we are interested in to generate holographic rough surfaces, such that the scattered field can be amplitude self-correlated. Until our best knowledge, almost all works related to the speckle pattern are irradiance correlated. However, in order to understand the physical features of the speckle pattern is necessary to obtain the amplitude correlation function, which must be manifested in the interference features between speckle motes. This is possible because for the same illumination configurations, the roughness parameters may obey two probability density functions. Other important effect occurs during the recording process, making possible to generate regions with cusped geometry. The behavior of the electric field in the neighborhood of these cusped regions generates evanescent waves [9,10], and it is used to generate surface plasmon fields. This occurs when a metal thin film is deposited on the holographic rough surface [11]. The surface plasmon fields appears when the power spectrum associated to the cusped region, is matched with the dispersion relation function of the surface plasmon. In the context of the angular spectrum model the cusped regions correspond to the Gibbs phenomenon [12].

The holographic rough surface proposed is generated by recording a set of optical fields kind cosine, the register media consists in a photo-resist film deposited on a glass substrate, using the periods of the optical field as the control parameter. This construction allows us to design the power spectrum of the holographic surface. Consequently, during the reconstruction process, the scattered field consists in a well localized speckle band.

The holographic rough surface thus generated is implemented as a beam splitter in an amplitude-correlation interferometer, which allows the interference between two speckle bands. The main feature is that the two speckle patterns coming from the same holographic rough surface obey different probability density functions; however a certain amplitude correlation function between the speckle patterns is preserved.

From the experimental results for the interference, very interesting features can be identified, one of them consists in the generation of bifurcation effects kind pitchfork [13,14]. The physical origin of this effect is explained from the boundary condition to the electromagnetic field. Since the theoretical point of view, the bifurcation effects allow to determinate the interaction between the irradiance distributions and can be interpreted as amplitude four order correlations. The geometry of the bifurcation suggests as application to be used as a kind of speckle tweezers. Another possible application consists in the alignment of nanoparticles and nanotubes inducing resonance effects close related to tunable spectroscopy [15-17]. Since the theoretical point of view, behavior such as Anderson localization can be implemented [18].

The structure of this chapter is as follows. In section *2*, we describe the synthesis of the rough surface, using as prototype cosine beams of different periods. When some consonance occurs between maximum or minimum values of the cosine beams, randomly distributed cusped points are generated. In the section *3*, we show the design of a very stable four arms interferometer by using the holographic rough surface as a beam splitter to generate two optical fields. In each arm, the optical field consists in a speckle pattern where each mote contains a set of cosine fringes. In section *4*, we show that controlling the size of the illumination beam, the mean size of the motes is also controlled, obeying an inverse relation, i.e. by decreasing the size of the illumination beam, the size of the mote increase. This property allows us to control the relative transversal separation between motes generating an interaction between interference fringes, the set of fringes presents similar behavior to wave-guide, allowing to explain the physical origin of the bifurcation effects. In section *5*, we describe the general conclusions remarking the property of the cusped points to generate surface plasmon fields and some potential applications are mentioned.

2. Holographic generation of rough surfaces

The holographic rough surfaces are generated by means of a superposition of cosenoidal patterns resulting of the interference between two plane waves, whose amplitude distribution is given by

http://dx.doi.org/10.5772/54512

$$\phi(x,z) = a\exp\left[ik\left(xsen\theta + z\cos\theta\right)\right] + a\exp\left[ik\left(-xsen\theta + z\cos\theta\right)\right], \tag{1}$$

where k is the wave number, θ is the incidence angle measured respect the normal vector n to the surface as it is sketched in Fig. 1.

The irradiance distribution takes the form

$$I(x,z) = \left|\phi(x,z)\right|^2 = 2a^2\left(1+\cos\left(kxsen\theta\right)\right). \tag{2}$$

By changing the incidence angle we generate a set of cosine patterns

$$I_q(x,z) = \left\{S_q\left(1+\cos\left(kxsen\theta_q + \delta_q\right)\right)\right\}. \tag{3}$$

with q=1,2,…n and S_q=2a_q^2. The phase term δ_q appears when a lateral shift in the maximum values is implemented.

These irradiance distributions are recorded on the holographic material. The experimental details are as follows. The holographic plate was made by depositing a photo-resist film using a spin-coating technique on a glass substrate. The number of irradiance distributions recorded were N=300 and it was excited using a *He-Cd* laser with a wavelength of 442 *nm*.

Assuming a lineal response of the holographic material, the mathematical representation to the resultant profile is

$$h(x) \approx \sum_{i=1}^{N}\left[1+\cos\left(K_n x + \delta_n\right)\right]S_n. \tag{4}$$

By considering that S_n is a random variable that depends on the exposition time of each register, and δ_n is a random phase controlled by shifting the holographic plate along the x-coordinate, then the holographic surface acquires a one dimensional random profile, whose height distribution satisfies a Gaussian probability density function as a consequence of the limit central theorem.

The transmittance function associated to the holographic surface is obtained by normalizing the height distribution in Eq. (4), and it is given by

$$t(x) = h(x) - \sum_{i=1}^{N} S_n = \sum_{i=1}^{N} S_n \cos\left(K_n x + \phi_n\right). \tag{5}$$

The statistical parameters of the surface are the following, the mean value of the rough surface profile is $\langle t(x)\rangle=0$.

The variance of the height distributions is given by

$$\sigma^2 = \frac{1}{2}\sum_{i=1}^{N} S_n^2. \tag{6}$$

Another important parameter is the length of correlation. This can be obtained following the classical definition of correlation, but it implies to lose the geometrical point of view, for this reason, we prefer to use an approximated relation. This can be done by noting that the maximum correlation of a cosine term with itself is $\pi/2$; with this interpretation, the correlation length depends geometrically on the initial and final recording angles, and can be expressed as

$$\Delta x = x_0 - x_0^{'} = \frac{\lambda}{4}\left(\frac{1}{sen\theta_i} - \frac{1}{sen\theta_f}\right). \tag{7}$$

Equations (5-7) are the expressions that carry on the information of the statistical properties of the holographic rough surface.

To generate the surface, we use a holographic system as it is sketched in Fig. (1). The mirrors and the holographic plate are placed on displacement mountings whose movements are controlled with a computer. This setup allows us to control the fringe period and the phase term δ_n. The recording times are random variables with uniform probability density function in the interval [0,2] sec., and it is controlled with the shutter shown in Fig. (1).

As a final remark of this section, during the recording process, some regions with geometrical cusped may be generated by the consonance in the maximum/minimum values of the cosine terms, as it is shown in Fig. 2.

The importance of these cusped regions appears during the reconstruction process, because they have the capacity to generate evanescent waves. We consider that the number of cusped regions follows a Poisson distribution. The amplitude value to the electric field in the neighborhood of these points can exceed in several magnitude orders the value respect other regions.

So far we have described the synthesis of holographic rough surfaces with controlled statistical parameters. To understand the physical features of the scattered field is necessary to study the amplitude distribution, this can be done by analyzing the interference effects as it is described in the following section.

http://dx.doi.org/10.5772/54512

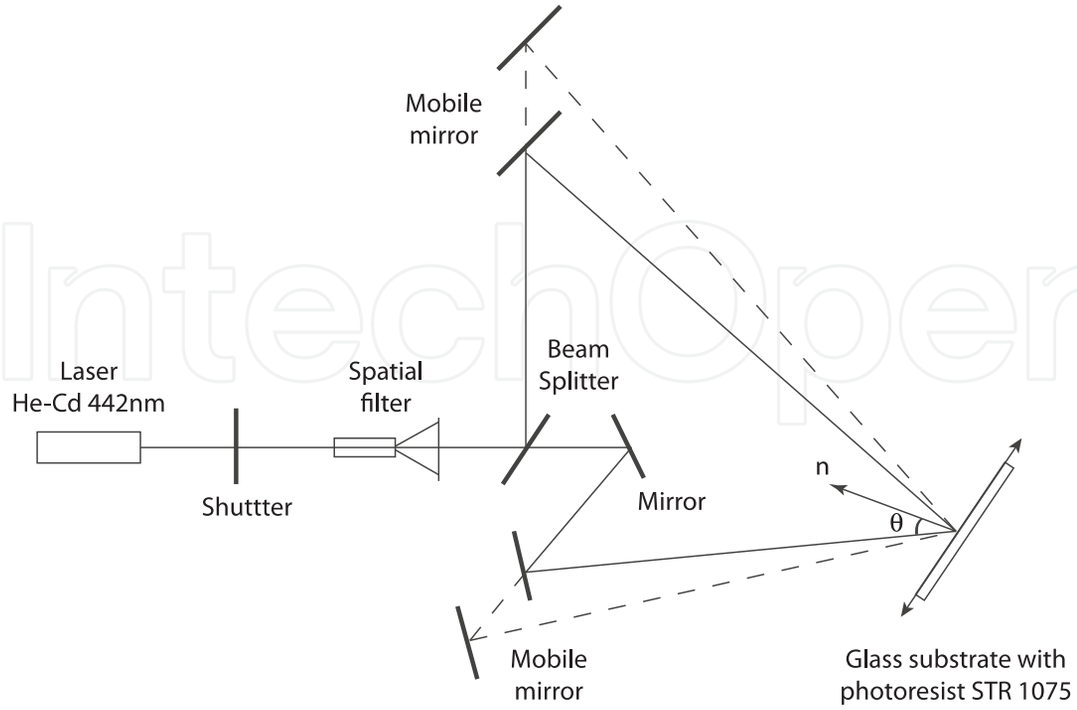

Figure 1. Schematic set up to generate the holographic rough surface.

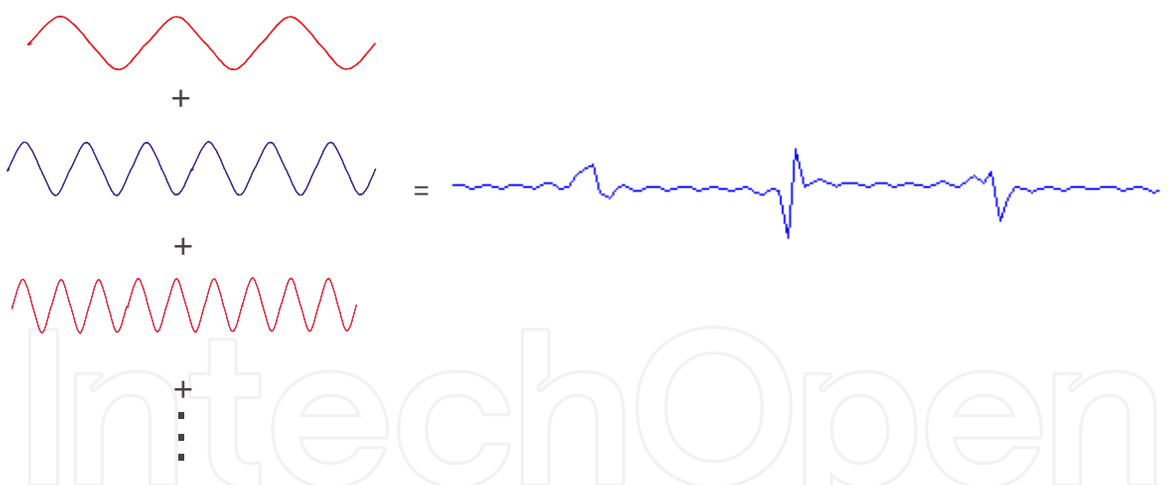

Figure 2. Consonance between maximum/minimum values of the cosine beams to generate cusped points.

3. Interference between speckle patterns

During the reconstruction process, the scattered field emerging from the rough surface, when it is illuminated with a plane wave has the structure of a speckle pattern. The speckle pattern is spatially bounded as a consequence of the recording process. This is because the recording incident angles of the plane waves take values in an established range, for the presented case

the angular range is *[30º-45º]*. However, the reconstruction wavelength used was of 632.8 *nm* emerging from a He-Ne laser.

It is a knowing fact that the amplitude function of a speckle pattern satisfies a Gaussian probability density function, and the irradiance distribution follows an exponential function [19]. In both cases, the statistical parameters such as the variance can be controlled with the transversal size of the illumination beam. This parameter will be used to control the bifurcation effects generated during the interference process, as it is shown below.

The holographic rough surface is implemented as a beam splitter to perform a four arm interferometer as it is sketched in Fig.3.

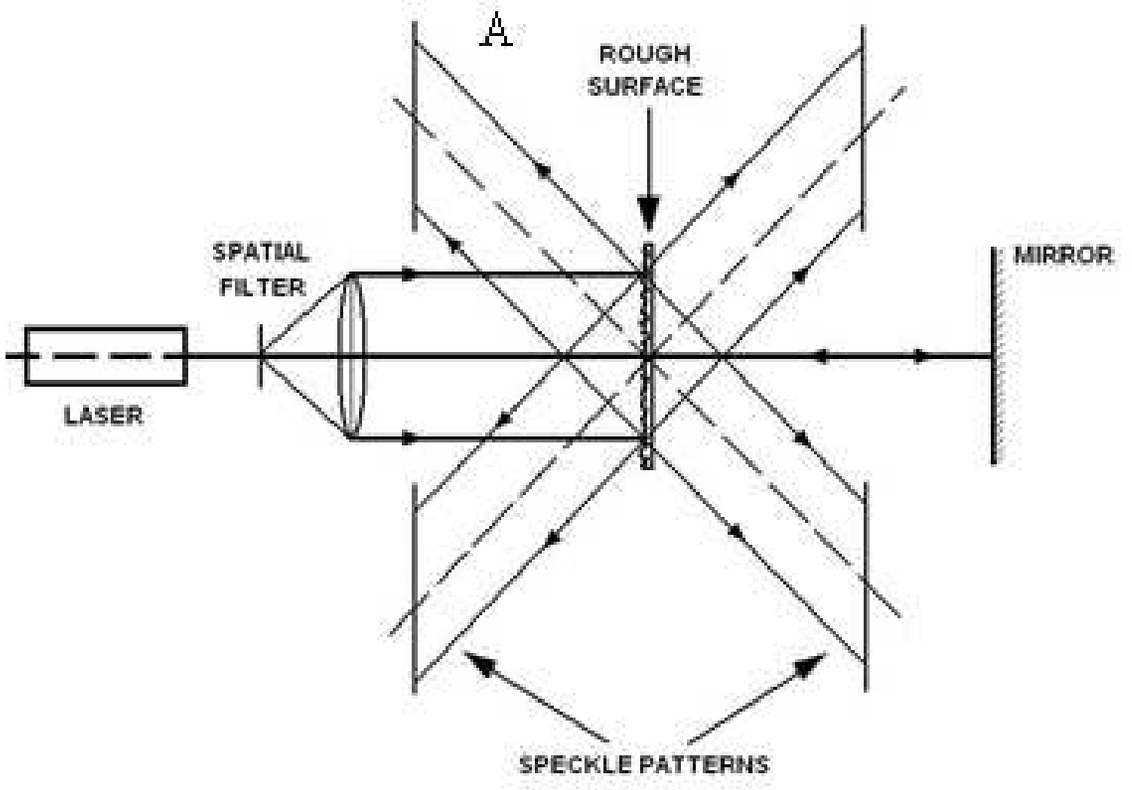

Figure 3. Experimental set up to generate the interference between speckle patterns.

The interference effects, on the arm *A* are generated by means of the amplitude superposition between the field emerging by reflection and the field emerging by the illumination of the zero order diffraction reflected in the mirror. Both fields are shifted each other, because the mean thickness of the holographic rough surface and the difference of the wavelengths. Then we have that, the structure of the interference pattern is locally similar to the Young experiment. This comment is reinforced by the experimental results showed in Fig4. In Fig. 4.a we show the speckle pattern and in Figs. 4.b, 4.c, we show the interference between two amplitude correlated speckle patterns for two configurations of illumination.

http://dx.doi.org/10.5772/54512

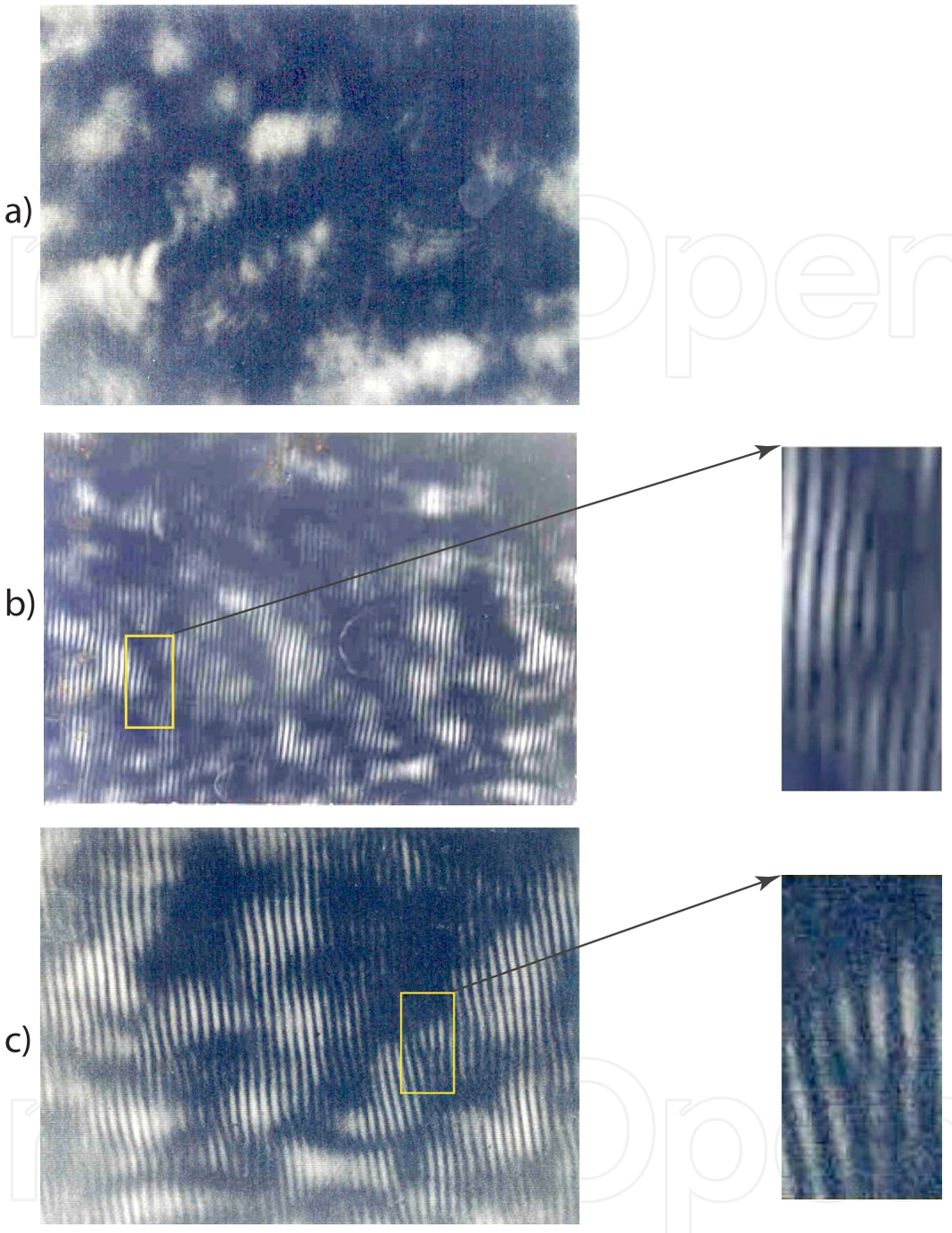

Figure 4. a) Speckle pattern generated by illuminating a rough surface with bounded power spectrum. The image was amplified *400X* using a microscope. b) and c) Interference between speckle patterns for two configurations of illumination. In both cases, the interference pattern presenting bifurcation effects kind pitchfork.

The expression for the interference is described as follows. The amplitude on an arbitrary point P is given by

$$\phi(P) = \phi_r(P) + \phi_t(P), \tag{8}$$

where the amplitude terms for reflected and transmitted fields can be approximated as

$$\begin{aligned}\phi_r(P) &\approx \sum_{n=1}^{N} A_n \exp\left[ikr_{np}\right] \\ \phi_t(P) &\approx \sum_{i=1}^{M} A_i \exp\left[ikr_{ip}\right].\end{aligned} \tag{9}$$

An important parameter is the number of trajectories N, M emerging from each surface, which in general are different because each optical field obey different probability density functions, this due to the zero order diffraction after reflection in the mirror illuminates the holographic rough surface with a wavelength of λ_t, this is a consequence of the propagation in a media with a refractive index corresponding to the holographic material.

The irradiance associated to the scattered field, takes the form

$$I(P) = \left|\phi_r(P)\right|^2 + \left|\phi_t(P)\right|^2 + 2\mathrm{Re}\,\phi_r(P)\phi_t^*(P), \tag{10}$$

and the mean irradiance is given by

$$\left\langle I(P)\right\rangle = \left\langle \left|\phi_r(P)\right|^2 \right\rangle_r + \left\langle \left|\phi_t(P)\right|^2 \right\rangle_t + 2\mathrm{Re}\left\langle \phi_r(P)\phi_t^*(P)\right\rangle. \tag{11}$$

A remarkable feature is that the interference area is controlled by means of the size of the illumination beam. This means that the N and M parameters in the sum term in Eq. (9) have an implicit dependence on the number of trajectories emerging from each holographic rough surface as sketching in Fig. 5.

The fact that the holographic rough surface exhibits two probability density functions is easily understood because the roughness profile is depending on the illumination wavelength. When the illuminating light is coming from free space, the probability density function for the amplitude field is $f(x,\lambda_0)$, and for the light reflected in the mirror through the photo-resist, the probability density function is $f_t(x,\lambda_t)$, meaning that both functions have the same functional dependence except a scale factor associated to the wavelength. This justifies that the scattered fields, given by Eq. (9), must present a certain correlation between the amplitude functions allowing the interference effects.

The average size of the speckle pattern is greater for the scattered field generated by reflection, this is because the refractive index, expressed as quotation between the wavelength implies that $n=\lambda_0/\lambda$. The typical values for the photo-resist refractive index are in the range [1.5-1.7]. A consequence of this fact is $\lambda_t<\lambda_0$.

http://dx.doi.org/10.5772/54512

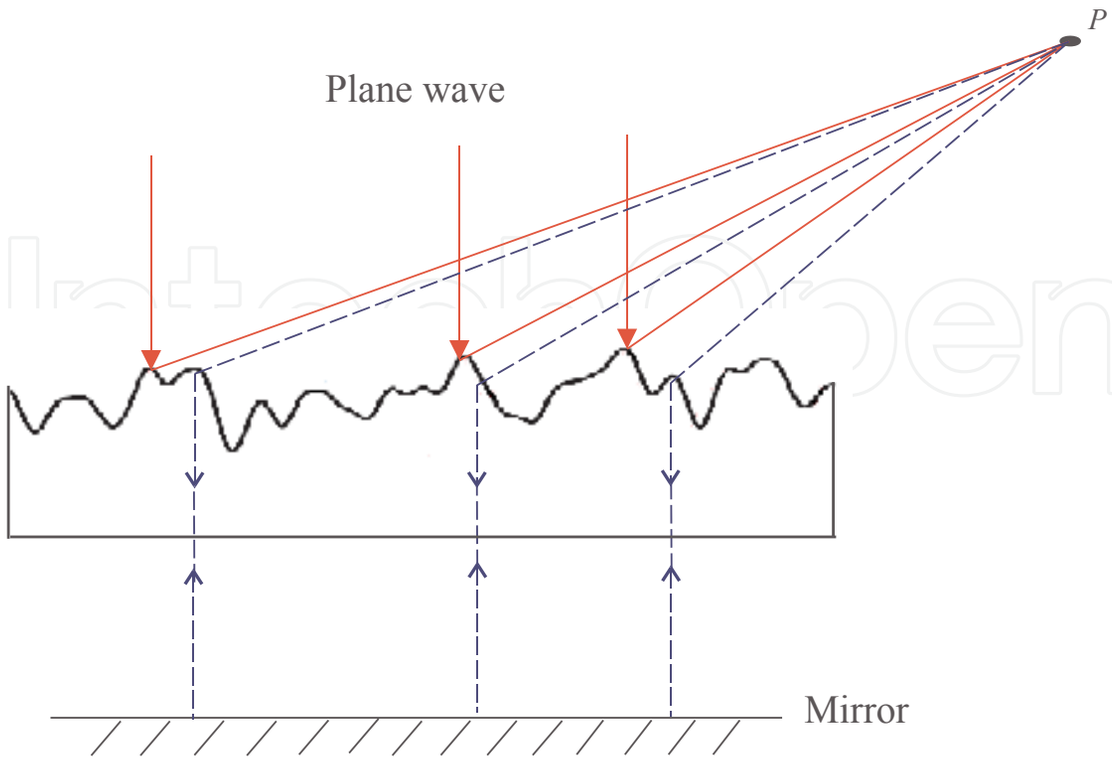

Figure 5. Generation of the interference effects on an arbitrary point *P*. The bold line represents light generated by the reflection on the rough surface coming from free space. The dot lines represent light from rough surface coming from the holographic media. The number of trajectories that arrives to point *P* may be different in each case.

The sub-index in the square brackets in Eq. (11) means that the mean value for the interference term must be calculated using the joint probability density function, which is an unknown function. However an approximate expression can be proposed by noting that one of the amplitude values can be scaled, such that the mean interference term may be calculate by using a Gaussian probability density function whose arguments depends on the relative difference between two arbitrary points $(x_2\text{-}x_1)$. This previous comments allows to describe completely the interference effects.

As a finally remark, by a visual analysis of the interference pattern it is easily to detect the existence of regions where the interference fringes are "branched", which corresponds to the bifurcation effects under study. The experimental shown in Fig. 4 are for normal incidence illumination and for angle of 5^o respect the normal n.

4. Description of bifurcation effects

The bifurcation effects are generated when one or more parameters that characterize the system change continually, such that, when they acquire some critical value, modify and generate new physical properties of the system. For the present study, this parameter is the size of the transversal section of the illumination beam, which allows controlling the size of the speckle

motes and then generates in a controlled way a transversal interaction between two or more speckle motes. The influence of this parameter is implicit in the number of trajectories N and M given in Eq. (9) that emerges from the rough surface and arrives on the same point p in the scattered field generating the interference effects. Each speckle mote has associated an interference fringes pattern, and the bifurcation effects are associated to the changes in the interference fringes when two or more speckle motes becomes closer. These comments are sketched in Fig. 6. In Fig. 6.a) we sketch two speckle motes, where the cosine interference fringes are bounded by the size and geometry of the mote. The size of the motes is controlled by changing the transversal size of the illumination beam, when this decreases, the size of the motes increase, and vice versa, as it is sketched in Fig. 6.b).

The transversal interaction between the interference fringes bounded by the speckle motes is shown in Fig. 6.c). The interaction between two interference fringe is the responsible of the generation of the bifurcation effects. The physical origin of this effect is in the boundary condition of the electromagnetic field which are dependent on the phase value in the contact point, in general, exists a discontinuity in the phase value when the interference fringes becomes closer. In order to satisfy the continuity of the tangential components of the electric field and the normal components of the electric displacement, a balance in energy and phase between the interference fringes occurs. This means that, when the two motes are far away no interaction occurs, when they become closer part of the energy must be transferred between the fringes, i.e. the energy flows through the fringes acquiring a final equilibrium value, modifying the interference fringes geometry. In general the fringes associated to each mote has different values in the phase function, which means that the fringes are shifted one respect to other. When a jump in the phase value of $\pi/2$ occurs between two fringes, geometrically means that a bright fringes is aligned with a dark fringes, the capacity of energy transfer is maximum, and the interference fringes splits generating the bifurcation effects kind pitchfork sketched in Fig. 6.c). This explanation agrees with the electromagnetic models and it is supported by the experimental results shown in Fig. 4.

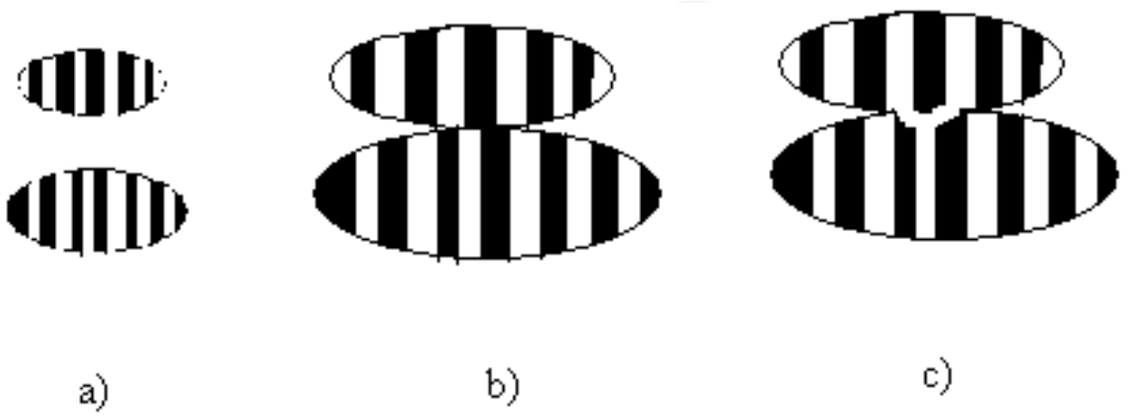

Figure 6. Description of bifurcation effects. In a) The two motes are independent and no interaction between the interference fringes occurs. In b), and c), when the motes become closer, an interaction between the fringes occurs unfolding the fringes structure. The splitting of the fringes is a consequence of the continuity of the electromagnetic field.

http://dx.doi.org/10.5772/54512

To describe the transversal interaction between interference fringes, we assume that two speckle neighborhood motes has irradiance I_1 and I_2 respectively, the energy transfer satisfies

$$\begin{aligned} \nabla_{\perp} I_1 &= \boldsymbol{a} I_2 \\ \nabla_{\perp} I_2 &= \boldsymbol{b} I_1, \end{aligned} \tag{12}$$

where $\nabla_{\perp} = \left(\hat{i} \frac{\partial}{\partial x} + \hat{j} \frac{\partial}{\partial y} \right)$ and $\boldsymbol{a}, \boldsymbol{b}$ are coupling constants vectors, in general case, $\boldsymbol{a}, \boldsymbol{b}$ may be function of position and time whose analysis is out scope of the present work. This two expressions are equivalent to have a single Helmholtz equation given by

$$\nabla^2 \left(I_1 - I_2 \right) = \left(\boldsymbol{a} \cdot \boldsymbol{b} \right) \left(I_1 - I_2 \right). \tag{13}$$

The nature of the solutions for the Helmholtz equation, depends on the difference between the irradiance values on a contact point, also as the sign of the dot product between the coupling vectors. The simplest case occurs when $\boldsymbol{a}.\boldsymbol{b} = 0$ corresponding to orthogonal polarization states. For this case, the Eq. (13) acquires the form of Laplace Equation and no interaction between irradiance distributions is expected.

When the dot product is negative, $\boldsymbol{a}.\boldsymbol{b} < 0$ the equation corresponds to the traditional Helmholtz equation used in classical optics. The physical implication is that, the interference fringes may be extended on a bigger region, because energy can flows troughs the interference fringes and the optical field presents a wave behavior, this effect corresponds to the interference fringes which are easely identified in Fig.(4).

When the dot product is positive, $\boldsymbol{a}.\boldsymbol{b} > 0$ the solutions has a decreasing exponential solution in some coordinate, i.e. the solution may have a wave behavior along one coordinate and an exponential decreasing in the other coordinate, this kind of solution, delimits a well identified interference region. All previous comments are in well agreement with the experimental results shown in Fig.4.

The study presented offers the possibility to generate local optical vortex by controlling in an alternating way the size of the illuminating beam, i.e. we pass from regions with bifurcation to region without bifurcation, controlling locally the geometry of the interference fringes. An important application of this effect is the possibility to transfer angular moment to particles placed in the neighborhood of the contact point of two speckle motes.

5. Final remarks and conclusions

In order to have a complete description of the scattered field generated by the holographic rough surface is necessary to describe the optical field emerging from the neighborhood of the cusped points. We approximate the effects by noting that the cusped point can be consider as

a quasi-point source, its representation, using the angular spectrum model, can be obtained using the Weyl representation given by [10]

$$\frac{\exp\left[ikr\right]}{r} = \frac{ik}{2\pi}\int_{-\infty}^{\infty}\frac{1}{m}\exp\left[ik\left(xu+yv+zp\right)\right]dudv, \tag{14}$$

where (u,v,p) are the spatial frequencies that satisfies

$$u^2+v^2+p^2 = \frac{1}{\lambda^2}. \tag{15}$$

It must be noted that the representation consists in two kinds of waves. One of them occurs when $u^2+v^2 \leq \frac{1}{\lambda^2}$ and it corresponds to homogeneous plane waves. Another case occurs when $u^2+v^2 > \frac{1}{\lambda^2}$, the spatial frequency p associated to the z-coordinate becomes imaginary, this corresponds to evanescent waves. More details concerning this representation can be founded in [10]. This evanescent character is implemented to generate other interesting physical features such as enhanced backscattering. When the holographic rough surface is covered with a metal thin film, the evanescent waves induce surface charge oscillations that propagate along the surface as a non-radiative inhomogeneous wave. These waves are known as surface plasmon waves. The important parameter is the relative separation between to cusped points. Then we have that incident light on the surface is coupled with the power spectrum of the cusped point generating a surface plasmon field. The propagation of the surface plasmon field when it meets another cusped point generates radiative optical field. This field interferes constructively with the incident light, this effect is known as enhanced backscattering, more detailed information to this effect can be found in [11].

In general the surface plasmon waves propagate short distances, typically 100 μm. [20], however long range surface plasmon waves can be generated by controlling the thickness of the metal film. When the thickness is in the range *[20 nm-60 nm]*, the length of propagation can reach until to 2000 μm [21], this allows to implement a two-dimensional surface plasmon optics. We assume that the thickness of the film does not change the roughness statistical parameters. The parameter that determinates the length of propagation of the surface plasmon is known as the dispersion relation function. For a semi-infinite media it is given by

$$\beta = \frac{\omega}{c}\left(\frac{\varepsilon_1\varepsilon_2}{\varepsilon_1+\varepsilon_2}\right)^{1/2}, \tag{16}$$

http://dx.doi.org/10.5772/54512

and for a metal thin film of thickness *[20 nm-60 nm]*, it acquires the form

$$\beta = \frac{\omega}{c}\left\{\left(\frac{\varepsilon_1\varepsilon_2}{\varepsilon_1+\varepsilon_2}\right)^{1/2} + 2an_1\left(\frac{\varepsilon_1\varepsilon_2}{\varepsilon_1+\varepsilon_2}\right)^{-1/2}\exp\left[-2\alpha d\right]\right\}. \tag{17}$$

From last representation, we have that to generate the coupling of illumination light-surface plasmon fields-scattered light, the mean distance between two cusped points L_c must be less than the length propagation of the plasmon field, i.e. $L_c < \beta^{-1}$, which is a necessary condition to improve the enhanced backscattering.

As a conclusion, in this chapter, we described the generation of a holographic rough surface using an incoherent convergence of holograms kind cosine. The surface was implemented to perform an interferometer that allows correlating two speckle patterns. The structure of the interference fringes shows the generation of bifurcation effects kind pitchfork. The splitting of the interference fringes is related with the size of the speckle motes and it is a consequence of the boundary conditions of the electromagnetic field. The superposition of cosine patterns generates cusped points randomly distributed and during the reconstruction process this cusped points generates evanescent waves. When the holographic rough surface is covered with a metal film, the cusped points generate surface plasmon fields.

Author details

G. Martínez Niconoff[1], G. Díaz González[1], P. Martínez Vara[2], J. Silva Barranco[1] and J. Munoz-Lopez[1]

1 Instituto Nacional de Astrofísica Óptica y Electrónica, Luis Enrique Erro No. , Tonantzintla, Puebla, México

2 Benemérita Universidad Autónoma de Puebla, Ciudad Universitaria, Facultad de Ingenierías, Puebla, México

References

[1] Hariharan, P. (1983). Colour Holography, *Progress in optics* 20, North-Holand, Amsterdam.,, 263-324.

[2] Yamaguchi, I, Ida, T, Yokota, M, & Yamashita, K. (2006). Surface shape measurement by phase-shifting digital holography with a wavelength shift. *Appl. Opt*. 45, , 7610-7616.

[3] Weidong MaoYongchun Zhong, Jianwen Dong, and Hezhou Wang, ((2005). Crystallography of two-dimensional photonic lattices formed by holography of three noncoplanar beams. *JOSA B*, 22(5), , 1085-1091.

[4] Matsushima, K. (2005). Computer-generated holograms for three-dimensional surface objects with shade and texture. *Appl. Opt*. 44, , 4607-4614.

[5] Parshall, D, & Kim, M. K. (2006). Digital holographic microscopy with dual-wavelength phase unwrapping. *Appl. Opt*. 45, , 451-459.

[6] Martinez-niconoff, G. Ramirez San Juan J.C., Muñoz-Lopez J., Martinez-Vara P., Carbajal-Dominguez A., and Sanchez-Gil J.A., ((2008). Spatial filtering dark hollow beams. *Opt. Comm*., 281 , 3237-3240.

[7] Korolev, E. (1996). Dynamic holography in alkali metal vapour. *Optics and Laser Technology*, 28(4), , 277-284.

[8] Demetri PsaltisFai Mok, and Hsin-Yu Sidney Li, ((1994). Nonvolatile storage in photorefractive crystals. *Opt. Lett*. 19, , 210-212.

[9] Jackson, J. D. (1998). *Classical Electrodynamics.* 3rd. Edition, *John Wiley & Sons, Inc., New York*, 047130932, 29-47.

[10] Mandel, L, & Wolf, E. (1995). *Optical Coherence and Quantum Optics.* Cambridge University Press., 0-52141-711-2, 120-125.

[11] West, C. S, & Donnell, K. A. O. (1995). Observations of backscattering enhancement from polaritons on a rough metal surface. *J. Opt. Soc. Am*. A,12, , 390-397.

[12] Shizgal, B, & Jung, J. H. (2003). Towards the Resolution of the Gibbs Phenomena, *J. Comput. Appl. Math*. 161, , 41-65.

[13] Beltrami, E. J. (1987). *Mathematics for dynamic modeling*. 2nd Edition, New York, *Academic Press Inc*. 0-12085-555-0, 171-202.

[14] Jyoti Champanerkar and Denis Blackmore(2007). Pitchfork bifurcations of invariant manifolds, *Topology and its Applications*., 154, , 1650-1663.

[15] Tal, R. V, Roze, G. A, Shandryuk, A. S, Merekalov, A. M, & Shatalova, O. A. Otmakhova, ((2009). Alignment of Nanoparticles in Polymer Matrices. *Polymer Science*, Ser. A 51, , 1194-1203.

[16] Miguel, A. Correa-Duarte, Marek Grzelezak, Veronica Salgueiriño-Maceira, Michael Giersig, Luis M.Liz-Marzan, Michael Farle, Karl Sierazdki, and Rodolfo Diaz, ((2005). Alignment of Carbon Nanotubes under Low Magnetic Fields through Attachment of Magnetic Nanoparticles. *J. Phys. Chem. B* 109 (41), , 19060-19063.

[17] Nahum Gat(2000). Imaging Spectroscopy Using Tunable Filters: A Review. *Proc. Spie* , 4056, 50-64.

[18] Sheng, P. (1991). Scattering and Localization of Classical Waves in Random Media,World Scientific, Singapore.

[19] Goodman, J. P. (1985). *Introduction to statistics optics*. John Wiley & Sons, 0-47101-502-4, 7-55.

[20] Raether, H. (1988). Surface plasmons on smooth and rough surfaces and on gratings. of *Springer tracts in modern physics*, Springer-Verlag, Berlin, 3-54017-363-2, 111, 4-37.

[21] Martínez, G, Niconoff, P, Martínez-vara, J, Muñoz-lopez, J. C, Juarez, M, & Carbajal-domínguez, A. (2011). Partially coherent surface plasmon modes. *Journal of the European Optical Society* 6,1109, , 1-6.

IntechOpen